Photoionization of hydrogen in a strong static electric field

Shun Ohgoda,[1] Oleg I. Tolstikhin,[2] and Toru Morishita[3,1]

[1]*Department of Engineering Science, The University of Electro-Communications, 1-5-1 Chofu-ga-oka, Chofu-shi, Tokyo 182-8585, Japan*

[2]*Moscow Institute of Physics and Technology, Dolgoprudny 141700, Russia*

[3]*Institute for Advanced Science, The University of Electro-Communications, 1-5-1 Chofu-ga-oka, Chofu-shi, Tokyo 182-8585, Japan*

(Received 19 February 2017; published 20 April 2017)

We analyze photoionization of hydrogen in the presence of a strong static electric field $F \sim 0.1$ a.u. Such a field essentially modifies the spectrum of the unperturbed atom. Even the ground $n = 1$ state acquires a non-negligible width, while the higher field-free bound states become overlapping resonances. At the same time, static-field-induced states (SFISs) found recently [A. V. Gets and O. I. Tolstikhin, Phys. Rev. A **87**, 013419 (2013)] emerge in the field-free continuum. We formulate the theory of photoionization from a decaying initial state and define appropriate observables—the reduced photoionization rate and transverse momentum distribution of photoelectrons. These observables are calculated for the four initial states with $n = 1$ and 2 in the different polarization cases. The SFISs are shown to manifest themselves as distinct peaks in the observables. Remarkably, even broad SFISs can be seen as narrow well-pronounced peaks at fields where their widths are comparable to that of the initial state. Such a resonance enhancement of the manifestations of SFISs is the main finding of this paper. This finding suggests that SFISs should manifest themselves also in photoelectron momentum distributions produced by photoionization in the presence of a quasistatic field of intense low-frequency laser pulses currently used in strong-field physics.

DOI: 10.1103/PhysRevA.95.043417

I. INTRODUCTION

Early experiments on photoionization of atoms in the presence of a static electric field were conducted with rubidium [1,2] and hydrogen [3–5]. The field strengths considered were in the range 1–15 kV/cm (2×10^{-7}–3×10^{-6} a.u.). Such fields are regarded as strong on the scale of static fields accessible in laboratory, but are several orders of magnitude weaker than typical field amplitudes ($\sim$0.1 a.u.) of intense low-frequency laser pulses currently used in strong-field physics [6]. The experiments revealed a reach field-induced structure in photoionization cross sections above the field-free ionization threshold, which has motivated numerous theoretical studies [7–12]. The structure consists of a series of rather broad peaks the positions and widths of which strongly depend on the field. Theoretical calculations of Stark states in hydrogen [12] quantitatively reproduce the peaks, which proves that they are manifestations of highly excited bound states ($n \sim 25$) promoted to positive energies and broadened by the field.

More recent experiments with lithium [13,14], hydrogen [15], and helium [16] supported by preliminary theoretical calculations [17–19] have raised a renewed interest in the subject. These experiments implemented the idea of the photoionization microscope [20]. The process considered is again photoionization of atoms in a static electric field, but the observable is different. The distribution of ionized electrons in the transverse to the static field plane was measured, which complements the information provided by the photoionization cross section. If the frequency of the ionizing field is tuned in resonance with one of the high-lying Stark states, this distribution was shown to rapidly change its shape compared to the off-resonance case and give an image of the wave function of the state. The static fields $\sim$1 kV/cm used in Refs. [13–16] are also weak compared to fields considered in strong-field physics.

In this paper we consider photoionization in really strong static fields of order $\sim$0.1 a.u. The range of fields is dictated and our interest in the subject is motivated by possible applications in strong-field physics. In the adiabatic regime, that is, at sufficiently low frequency and high intensity of a laser pulse, the interaction of an atom with the electric field of the pulse proceeds as if the field were static and equal to its instantaneous value [21]. Irradiating an atom interacting with such a quasistatic field of a strong pump pulse by a weak high-frequency probe pulse should enable one to extend the previous studies of photoionization in an electric field [1–5,13–16] to much stronger fields. This, in particular, may provide access to the study of the recently found static-field-induced states (SFISs) [22], which would open a new avenue of research in strong-field physics.

Our goal is to find manifestations of SFISs in photoionization of hydrogen in a strong laser field. We approach this goal in two steps. In the present paper we consider photoionization in a truly static field. This is needed because photoionization observables in a quasistatic field within the adiabatic theory [21] can be expressed in terms of their static-field counterparts. In the second part of the study to be reported elsewhere the present static-field results will be used to describe photoionization in a slowly varying field of an intense low-frequency laser pulse.

The paper is organized as follows. The theory is presented in Sec. II. We first discuss how an external static electric field modifies the spectrum of hydrogen (Sec. II A), giving a brief review of tunneling states, which are field-free bound states shifted and broadened by the field, and SFISs, which emerge in the field-free continuum [22]. Then we introduce observables for photoionization in a strong electric field (Sec. II B). The results of illustrative calculations are presented in Sec. III. Section IV concludes the paper. Some details of our numerical procedure are discussed in the Appendix.

II. THEORY

A. Tunneling and static-field-induced states

The Schrödinger equation for a hydrogen atom in a static uniform electric field $\mathbf{F} = F\mathbf{e}_z$, $F \geqslant 0$, reads (atomic units are used throughout)

$$\left[-\frac{1}{2}\Delta - \frac{1}{r} + Fz - E\right]\phi(\mathbf{r}) = 0. \tag{1}$$

We are interested in solutions which are regular at the origin and satisfy outgoing-wave boundary conditions in the asymptotic region $z \to -\infty$. Such solutions represent hydrogenic Siegert states (SSs) in an electric field [23]. Equation (1) is separable in parabolic coordinates [24]

$$\xi = r + z, \quad 0 \leqslant \xi < \infty, \tag{2a}$$

$$\eta = r - z, \quad 0 \leqslant \eta < \infty, \tag{2b}$$

$$\varphi = \arctan\tfrac{y}{x}, \quad 0 \leqslant \varphi < 2\pi. \tag{2c}$$

The SSs can be found in the form

$$\phi(\mathbf{r}) = \eta^{-1/2} f(\eta)\phi(\xi)\frac{e^{im\varphi}}{\sqrt{2\pi}}, \tag{3}$$

where $m = 0, \pm1, \pm2, \ldots$. The functions $\phi(\xi)$ and $f(\eta)$ satisfy

$$\left[\frac{d}{d\xi}\xi\frac{d}{d\xi} - \frac{m^2}{4\xi} + 1 - \beta + \frac{E\xi}{2} - \frac{F\xi^2}{4}\right]\phi(\xi) = 0, \tag{4a}$$

$$\phi(\xi)|_{\xi\to0} \propto \xi^{|m|/2}, \quad \phi(\xi)|_{\xi\to\infty} = 0, \tag{4b}$$

and

$$\left[\frac{d^2}{d\eta^2} + \frac{1-m^2}{4\eta^2} + \frac{\beta}{\eta} + \frac{E}{2} + \frac{F\eta}{4}\right]f(\eta) = 0, \tag{5a}$$

$$f(\eta)|_{\eta\to0} \propto \eta^{(|m|+1)/2}, \quad f(\eta)|_{\eta\to\infty} \propto f(\eta, E), \tag{5b}$$

where

$$f(\eta, E) = \frac{2^{1/2}}{(F\eta)^{1/4}}\exp\left(\frac{iF^{1/2}\eta^{3/2}}{3} + \frac{iE\eta^{1/2}}{F^{1/2}}\right). \tag{6}$$

The latter function for real E has unit outgoing flux at $\eta \to \infty$, which corresponds to $z \to -\infty$. Each of Eqs. (4) and (5) is an eigenvalue problem, so the solutions exist only for a discrete set of generally complex values of energy E and separation constant β. The SSs are normalized by [23]

$$\int \bar{\phi}(\mathbf{r})\phi(\mathbf{r})\,d\mathbf{r} = \frac{1}{4}\int_0^\infty\int_0^\infty \eta^{-1} f^2(\eta)\phi^2(\xi)(\xi+\eta)\,d\xi\,d\eta = 1, \tag{7}$$

where $\bar{\phi}(\mathbf{r})$ is given by Eq. (3) with the opposite sign of m. The function $f(\eta)$ exponentially diverges at $\eta \to \infty$ for $\mathrm{Im}\,E < 0$, so the integral over η should be regularized by rotating the integration path into the upper half of the complex η plane [23]. Our numerical procedure to construct the SSs is outlined in Sec. 1 of the Appendix.

The separable form (3) suggests that the eigenfunction $\phi(\mathbf{r})$ can be labeled by a set of parabolic quantum numbers (n_ξ, n_η, m), with $n_\xi = 0,1,2,\ldots$ and $n_\eta = 0,1,2,\ldots$ giving the numbers of zeros of the solutions of Eqs. (4) and (5), respectively. This is true for bound states, but does not generally apply to SSs, because the solutions in this case are complex and do not have definite numbers of zeros. We note that the term SS refers to all (infinitely many) solutions of Eqs. (4) and (5) at any field F. The eigenvalues E for the majority of SSs lie deep in the complex energy plane. However, there are situations where for some SSs they are located close to the real axis. The imaginary part of the solutions in this case is small compared to their real part, and then quantum numbers n_ξ and n_η acquire approximate nodal meaning. Only such SSs are observable individually.

One such situation is met if one considers what happens with bound-state solutions of Eq. (1) in the presence of a weak field. The field only slightly disturbs the solutions, so they approximately preserve their nodal structure and can be labeled by parabolic quantum numbers of the corresponding unperturbed bound state [24]. Their eigenvalue presented in the form

$$E = \mathcal{E} - \frac{i}{2}\Gamma \tag{8}$$

defines the Stark-shifted energy $\mathcal{E}$ and ionization rate Γ of the state. The states decay by tunneling through an effective potential barrier in Eq. (5a). Their energies and rates can be obtained as asymptotic expansions in F, where the coefficients are determined by the set (n_ξ, n_η, m) [24–26]. For each state there exists a critical field F_c at which the energy $\mathcal{E}$ passes trough the top of the barrier. The expansions hold only in the tunneling regime $F < F_c$, so such SSs are called tunneling states (TSs) [22]; they are also known as Stark states. In the tunneling regime quantum numbers n_ξ and n_η preserve their meaning and TSs are characterized by the following properties: (1) their wave functions are localized in the Coulomb potential well near the origin, (2) their energies $\mathcal{E}$ are negative, (3) their widths Γ are exponentially small in F and hence for sufficiently weak fields become smaller than the energy distance to the neighboring states, and (4) the leading-order term in the asymptotic expansion of the separation constant is

$$\beta|_{F\to0} = 1 - \varkappa\left(n_\xi + \frac{|m|+1}{2}\right), \tag{9}$$

where $\varkappa = \sqrt{-2E|_{F=0}} = 1/n$ and $n = n_\xi + n_\eta + |m| + 1$ is the principle quantum number. The energies and ionization rates of the four lowest TSs originating from bound states with $n = 1$ and 2 as functions of F are shown in the lower part of Fig. 1. These states are well separated in the tunneling regime. They can be analytically continued to the over-the-barrier regime $F > F_c$, where their widths rapidly grow and they begin to overlap. Quantum numbers n_ξ and n_η still can be used in this case to label the states, by continuity, but they lose their nodal meaning.

Another situation in which n_ξ and n_η acquire approximate meaning occurs when an electron bounces in a "resonator" formed by the Coulomb potential, on the one side, and the rising part of the field potential Fz in the region $z > 0$, on the other side. Since the resonator does not exist without an external electric field, the states trapped in it do not exist either, so they are called static-field-induced states [22]. SFISs decay by leaking through the Coulomb end of the resonator, because

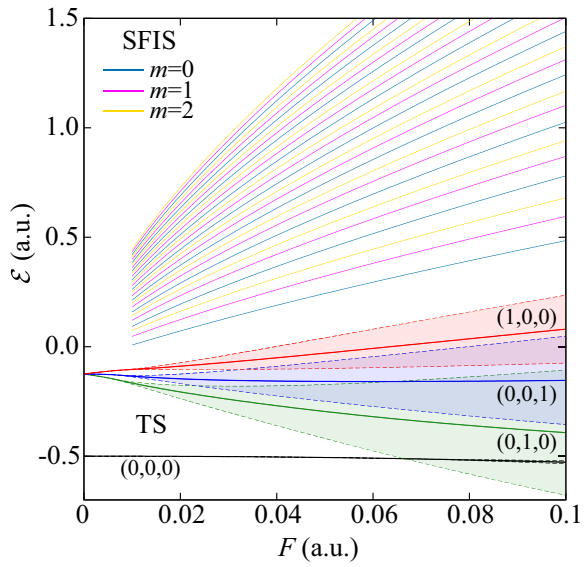

FIG. 1. Real parts of the energy eigenvalues, Eq. (8), for a number of TSs and SFISs relevant for the present discussion as functions of the field F. Four lowest TSs the photoionization of which is considered labeled by parabolic quantum numbers (n_ξ,n_η,m) are shown in the lower part of the figure. The shadowed areas around the curves indicate ionization rates Γ of the states. SFISs with quantum numbers $n_\xi = 2,\ldots,10$ (from bottom to top), $n_\eta = 0$, and $m = 0$, 1, and 2 are shown in the upper part of the figure.

of imperfect reflection, while reflection from the field end is complete. An asymptotic quantization condition for SFISs based on this physical picture was derived in Ref. [22]. For hydrogen, this condition reads

$$\frac{k^3}{3F}+\frac{i}{2}(b-a)\ln\frac{4k^3}{F}-\frac{i}{2}\ln\frac{\Gamma(b)}{\Gamma(a)}=\pi\left(n_\xi+\frac{|m|}{4}+\frac{1}{2}\right), \tag{10}$$

where $k=\sqrt{2E}$, $a=i/k-n_\eta$, and $b=1+|m|-a$. It implicitly defines the eigenvalues E as functions of the set (n_ξ,n_η,m). The characteristic properties of SFISs distinguishing them from TSs are: (1) their wave functions are localized in the resonator region which extends towards $z>0$ up to $z\sim\mathcal{E}/F$, (2) their energies $\mathcal{E}$ are positive, (3) their widths Γ are comparable to the energy spacing between them, and (4) the leading-order term in the asymptotic expansion of the separation constant in the weak-field case is

$$\beta|_{F\to 0}=-ik\left(n_\eta+\frac{|m|+1}{2}\right), \tag{11}$$

where k has a nontrivial dependence on F dictated by Eq. (10). The energies of a number of the lowest SFISs as functions of F are shown in the upper part of Fig. 1. The widths of SFISs rapidly grow with n_η [22], so we consider only states with $n_\eta = 0$. The results are obtained by finding the exact solutions of Eqs. (4) and (5) near the corresponding solutions of Eq. (10), which enables us to assign a definite set of quantum numbers (n_ξ,n_η,m) to each state. SFISs obtained in this way at a finite F can be analytically continued to zero field. We have done such calculations for a number of states. All the SFISs considered turn into TSs and then bound states as F decreases to zero. In this case, for each SFIS there exists a boundary field F_b below which the state is captured by the Coulomb potential, its energy $\mathcal{E}$ becomes negative, and the asymptotic quantization condition (10) ceases to apply [22]. This means that at $F<F_b$ quantum numbers n_ξ and n_η lose their meaning and are generally not conserved, that is, they may change in the evolution of a given SS from a SFIS to a TS as F decreases. This indeed happens; for example, the SFIS (1,1,0) turns into the TS (2,1,0) with an increment of n_ξ, but we did not find examples of such a behavior for states with $n_\eta = 0$. We mention that in the case of the zero-range potential there exists only one bound state, and hence only one SFIS turns into the only TS as F decreases. The eigenvalues E of all the other SFISs coalesce at zero; these states disappear and do not have counterparts at $F = 0$ [22]. It is clear that such disappearing SFISs should exist for any finite-range potential supporting only a finite number of bound states. They may exist also for the Coulomb potential, although we could not find them in the calculations, the analysis in this case being complicated by the infinite number of bound states.

TSs and SFISs do not complete a list of situations where quantum numbers n_ξ and n_η acquire approximate nodal meaning. Another situation of this type occurs when the energy $\mathcal{E}$ of an SS lies close to the top of the potential barrier in Eq. (5a). A uniform semiclassical quantization condition for such top-of-the-barrier states (TBSs) was derived in Ref. [27]. This condition and the underlying physical picture differ from those for both TSs and SFISs. The difference resulting in different dependencies of the eigenvalues E on quantum numbers (n_ξ,n_η,m) and field F is what eventually justifies the different names of the states. It can be said that TBSs are encountered on the way from TSs to SFISs as F grows. The results obtained from the quantization condition for TBSs [27] for states with $n\sim 25$ at field strengths $F\sim 10^{-6}$ used in experiments with hydrogen [3–5] are in good agreement with accurate calculations [12] which, in turn, closely reproduce positions and widths of peaks in the experimental photoionization cross sections. Using the present terminology, this means that the peaks observed in Refs. [3–5] are manifestations of TBSs. The goal of this paper is to investigate whether SFISs also reveal themselves as distinct peaks in photoionization observables at stronger fields $F\sim 0.1$.

B. Photoionization from a tunneling state

The spectrum of hydrogen modified by a strong static field F, as discussed above, can be probed by allowing the system to interact with a weak time-dependent field $\mathbf{f}(t)$ of an electromagnetic pulse. The interaction may result in photoionization. We are going to analyze photoionization from the four TSs shown in Fig. 1 in static fields $F\sim 0.1$. At such fields, even the lowest TS originating from the ground state acquires a non-negligible width, and the widths of the higher TSs exceed the energy spacing between them. It is natural to ask whether and how one can prepare such a rapidly decaying initial state for a photoionization experiment. This important question must be clarified before we continue. Our answer is: one probably cannot, if the experiment is to be performed with a truly static field F, as was the case in Refs. [1–5,13–16]. But intense low-frequency laser pulses provide a means to prepare such decaying states in a quasistatic field. Indeed, in

the adiabatic regime an initial bound state interacting with a strong laser field turns into the corresponding SS in a static electric field equal to the instantaneous value of the laser field and adiabatically follows the field [21]. By applying an additional probe field $\mathbf{f}(t)$, one can study photoionization from the SS. The static-field results presented in this paper are needed to describe photoionization in a strong laser field to be considered elsewhere.

1. Basic equations

The time-dependent Schrödinger equation describing the interaction with a weak probe field $\mathbf{f}(t)$ in the dipole approximation reads

$$i\frac{\partial\psi(\mathbf{r},t)}{\partial t}=\left[-\frac{1}{2}\Delta-\frac{1}{r}+Fz+\mathbf{f}(t)\mathbf{r}\right]\psi(\mathbf{r},t). \tag{12}$$

The field is expressed by the Fourier transform

$$\mathbf{f}(t)=\int\mathbf{f}(\omega)e^{-i\omega t}\frac{d\omega}{2\pi},\quad \mathbf{f}(\omega)=\mathbf{f}^*(-\omega). \tag{13}$$

The function $\mathbf{f}(\omega)$ for $\omega>0$ is presented as

$$\mathbf{f}(\omega)=f(\omega)\mathbf{e},\quad \mathbf{e}\mathbf{e}^*=1, \tag{14}$$

where $f(\omega)$ is the amplitude and $\mathbf{e}$ is the polarization vector at frequency ω. We will consider linear polarization (LP) and circular polarization (CP) cases defined by

$$\text{LP:}\quad \mathbf{e}=\mathbf{e}_z, \tag{15a}$$

$$\text{CP}(\pm):\quad \mathbf{e}=\frac{\mathbf{e}_x\pm i\mathbf{e}_y}{\sqrt{2}}. \tag{15b}$$

The eigenvalue and eigenfunction of the initial TS satisfying Eqs. (4) and (5) are denoted by $E_{\rm in}=\mathcal{E}_{\rm in}-\frac{i}{2}\Gamma_{\rm in}$ and $\phi_{\rm in}(\mathbf{r})$, respectively. The solution of Eq. (12) is sought in the form

$$\psi(\mathbf{r},t)=\phi_{\rm in}(\mathbf{r})e^{-iE_{\rm in}t}+\int\psi(\mathbf{r},\omega)e^{-iE_{\rm in}t-i\omega t}\frac{d\omega}{2\pi}. \tag{16}$$

Substituting this into Eq. (12) and treating the term with $\mathbf{f}(t)$ as a perturbation, in the first order we obtain an inhomogeneous time-independent equation defining $\psi(\mathbf{r},\omega)$,

$$\left[-\frac{1}{2}\Delta-\frac{1}{r}+Fz-E_{\rm in}-\omega\right]\psi(\mathbf{r},\omega)=-\mathbf{f}(\omega)\mathbf{r}\phi_{\rm in}(\mathbf{r}). \tag{17}$$

This function describes electrons released from the atom by photoionization at frequency ω. Whatever is the polarization of $\mathbf{f}(\omega)$, such electrons are eventually driven by the static field and fly away towards $z\to-\infty$, so $\psi(\mathbf{r},\omega)$ may have only outgoing waves in this asymptotic region. The corresponding solution of Eq. (17) can be obtained with the help of the outgoing-wave Green's function satisfying

$$\left[-\frac{1}{2}\Delta-\frac{1}{r}+Fz-E\right]G(\mathbf{r},\mathbf{r}';E)=\delta(\mathbf{r}-\mathbf{r}') \tag{18}$$

and is given by

$$\psi(\mathbf{r},\omega)=\mathbf{f}(\omega)\mathbf{D}(\mathbf{r},\omega), \tag{19}$$

where

$$\mathbf{D}(\mathbf{r},\omega)=-\int G(\mathbf{r},\mathbf{r}';E_{\rm in}+\omega)\mathbf{r}'\phi_{\rm in}(\mathbf{r}')\,d\mathbf{r}'. \tag{20}$$

Similar equations can be found, e.g., in Ref. [17]. However, there is one important difference: in our case the initial state in Eq. (20) is a TS which fully incorporates the effect of the static field in Eq. (12), while all previous theoretical studies on the subject [7–11,17–19] treated photoionization from an unperturbed bound state. This approximation is justified for the very weak fields considered there, but does not apply in the present case.

The function (20) defines all photoionization observables. Two objects are needed to obtain it: the initial TS discussed in Sec. II A and the Green's function. We first summarize equations defining the Green's function, and then turn to observables.

2. Green's function

A method to construct the Green's function is described in Ref. [17]. In the present case, we need this function for generally complex values of its energy argument. Here we outline the present procedure; details of its numerical implementation are deferred to Sec. 2 of the Appendix. The outgoing-wave solution of Eq. (18) can be found in the form

$$G(\mathbf{r},\mathbf{r}';E)=\frac{-2}{\sqrt{\eta\eta'}}\sum_\nu\mathcal{G}_\nu(\eta,\eta')\Phi_\nu(\xi,\varphi)\Phi_{\bar\nu}(\xi',\varphi'), \tag{21}$$

where

$$\Phi_\nu(\xi,\varphi)=\phi_\nu(\xi)\frac{e^{im\varphi}}{\sqrt{2\pi}} \tag{22}$$

are parabolic channel functions labeled by the multi-index [28]

$$\nu=(n_\xi,m),\quad n_\xi=0,1,\ldots,\quad m=0,\pm1,\ldots, \tag{23}$$

and $\bar\nu=(n_\xi,-m)$. The functions $\phi_\nu(\xi)$ are the solutions to the eigenvalue problem

$$\left[\frac{d}{d\xi}\xi\frac{d}{d\xi}-\frac{m^2}{4\xi}+1-\beta_\nu+\frac{E\xi}{2}-\frac{F\xi^2}{4}\right]\phi_\nu(\xi)=0, \tag{24a}$$

$$\phi_\nu(\xi)|_{\xi\to0}\propto\xi^{|m|/2},\quad \phi_\nu(\xi)|_{\xi\to\infty}=0. \tag{24b}$$

In contrast to Eq. (4), here E is assumed to be fixed and equal to the energy argument in Eq. (21) and the separation constant β_ν is treated as the corresponding eigenvalue. The different solutions of Eqs. (24) for given m, E, and F are enumerated by n_ξ in descending order of $\mathrm{Re}\,\beta_\nu$, as suggested by Eq. (9), and normalized by

$$\int_0^\infty\phi_{n_\xi m}(\xi)\phi_{n'_\xi m}(\xi)\,d\xi=\delta_{n_\xi n'_\xi}. \tag{25}$$

This leads to the normalization condition for parabolic channels

$$\int_0^\infty\int_0^{2\pi}\Phi_{\bar\nu}(\xi,\varphi)\Phi_{\nu'}(\xi,\varphi)\,d\xi\,d\varphi=\delta_{\nu\nu'}, \tag{26}$$

where $\nu' = (n'_\xi, m')$. The function $\mathcal{G}_\nu(\eta,\eta')$ is the outgoing-wave solution of

$$\left[\frac{d^2}{d\eta^2} + \frac{1-m^2}{4\eta^2} + \frac{\beta_\nu}{\eta} + \frac{E}{2} + \frac{F\eta}{4}\right]\mathcal{G}_\nu(\eta,\eta') = \delta(\eta-\eta'). \tag{27}$$

It can be found in the form

$$\mathcal{G}_\nu(\eta,\eta') = \mathcal{W}_\nu^{-1}\mathcal{R}_\nu(\eta_<)\mathcal{O}_\nu(\eta_>), \tag{28}$$

where $\eta_<$ ($\eta_>$) is the smaller (larger) of η and η'. The functions $\mathcal{R}_\nu(\eta)$ and $\mathcal{O}_\nu(\eta)$ are the regular and outgoing-wave solutions of the corresponding homogeneous equation, respectively, defined by the boundary conditions

$$\mathcal{R}_\nu(\eta\to 0) = \eta^{(|m|+1)/2} \tag{29}$$

and

$$\mathcal{O}_\nu(\eta\to\infty) = f(\eta,E), \tag{30}$$

where $f(\eta,E)$ is defined by Eq. (6), and $\mathcal{W}_\nu$ is their Wronskian,

$$\mathcal{W}_\nu = \mathcal{R}_\nu(\eta)\mathcal{O}'_\nu(\eta) - \mathcal{O}_\nu(\eta)\mathcal{R}'_\nu(\eta). \tag{31}$$

In the asymptotic region the regular solution takes the form

$$\mathcal{R}_\nu(\eta\to\infty) = \frac{e^{-3i\pi/4+i\delta_\nu}2^{1/2}\mathcal{W}_\nu}{(F\eta)^{1/4}} \times \sin\left(\frac{F^{1/2}\eta^{3/2}}{3} + \frac{E\eta^{1/2}}{F^{1/2}} + \frac{\pi}{4} + \delta_\nu\right), \tag{32}$$

where δ_ν is the phase shift in channel ν. The outgoing-wave solution $\mathcal{O}_\nu(\eta)$ is generally irregular at $\eta\to 0$. But it becomes regular if E coincides with one of the SS eigenvalues; in this case functions $\mathcal{R}_\nu(\eta)$ and $\mathcal{O}_\nu(\eta)$ become linearly dependent, their Wronskian (31) turns to zero, and $G(\mathbf{r},\mathbf{r}';E)$ as a function of E has a pole.

3. *Observables*

We now turn to photoionization observables. They are determined by coefficients appearing in the asymptotic form of $\mathbf{D}(\mathbf{r},\omega)$ at $\eta\to\infty$. Substituting Eqs. (21) and (28) into Eq. (20) yields

$$\mathbf{D}(\mathbf{r},\omega)|_{\eta\to\infty} = \eta^{-1/2}f(\eta,E_{\rm in}+\omega)\sum_\nu \mathbf{d}_\nu(\omega)\Phi_\nu(\xi,\varphi), \tag{33}$$

where

$$\mathbf{d}_\nu(\omega) = \frac{2}{\mathcal{W}_\nu}\int \eta^{-1/2}\mathcal{R}_\nu(\eta)\Phi_{\bar\nu}(\xi,\varphi)\mathbf{r}\phi_{\rm in}(\mathbf{r})\,d\mathbf{r} \tag{34}$$

are the coefficients in question. To clarify their physical meaning, let us temporarily assume that the field F is very weak. Then the energy $E_{\rm in}$ of the initial state is almost real and $f(\eta,E_{\rm in}+\omega)$ represents an outgoing wave with unit flux at $\eta\to\infty$. Substituting Eq. (33) into Eq. (19) decomposes the outgoing flux of photoelectrons into orthonormal parabolic channels, see Eq. (26), with the flux in channel ν given by $|\mathbf{f}(\omega)\mathbf{d}_\nu(\omega)|^2$. This quantity has the meaning of partial rate of photoionization in channel ν caused by the interaction with a weak monochromatic field of frequency ω, amplitude $f(\omega)$, and polarization $\mathbf{e}$. To eliminate the dependence on the amplitude, which is a property of the probe pulse, not the atom, we divide the rate by $|f(\omega)|^2$; the ratio

$$\gamma_\nu(\omega) = |\mathbf{e}\mathbf{d}_\nu(\omega)|^2 \tag{35}$$

is called the reduced partial ionization rate in channel ν. Summing up over all channels gives the reduced total ionization rate,

$$\gamma(\omega) = \sum_\nu \gamma_\nu(\omega). \tag{36}$$

In the following, for brevity, we omit the qualification "reduced". These rates constitute the first set of observables to be considered in the calculations. We note that $\gamma(\omega)$ differs by only an inessential factor from the photoionization cross section $\sigma(\omega)$ measured in Refs. [3–5] and considered theoretically in Refs. [7,8,10,11], namely, $\gamma(\omega) = \frac{c}{2\pi}\sigma(\omega)$. We prefer to discuss rates because of the similarity of the structure of the outgoing flux of electrons in the present problem to that in the problem of tunneling ionization in a static field [28], which is made use of below.

The function $\mathbf{D}(\mathbf{r},\omega)$ in the asymptotic region can be also presented in the form [28]

$$\mathbf{D}(\mathbf{r},\omega)|_{z\to-\infty} = \int \mathbf{A}(\mathbf{k}_\perp,\omega)e^{i\mathbf{k}_\perp\mathbf{r}_\perp}g(z,k_\perp)\frac{d\mathbf{k}_\perp}{(2\pi)^2}, \tag{37}$$

where $\mathbf{r}_\perp = (x,y) = (r_\perp\cos\varphi, r_\perp\sin\varphi)$, $\mathbf{k}_\perp = (k_x,k_y) = (k_\perp\cos\varphi_k, k_\perp\sin\varphi_k)$,

$$g(z,k_\perp) = e^{-i\pi/12}2\pi^{1/2}(2F)^{-1/6}\,\mathrm{Ai}(\zeta), \tag{38a}$$

$$\zeta = \frac{2e^{-i\pi/3}}{(2F)^{2/3}}\left[E_{\rm in}+\omega - Fz - \frac{k_\perp^2}{2}\right], \tag{38b}$$

and $\mathrm{Ai}(x)$ is the Airy function [29]. Equations (37) and (33) hold in the same region, which enables one to express $\mathbf{A}(\mathbf{k}_\perp,\omega)$ in terms of $\mathbf{d}_\nu(\omega)$. Reproducing the derivation given in Ref. [28], we obtain

$$\mathbf{A}(\mathbf{k}_\perp,\omega) = \frac{2^{3/2}\pi i}{F^{1/2}}\sum_\nu \mathbf{d}_\nu(\omega)\Phi_\nu\left(\frac{k_\perp^2}{F},\varphi_k\right). \tag{39}$$

The meaning of $\mathbf{A}(\mathbf{k}_\perp,\omega)$ is that the product $\mathbf{f}(\omega)\mathbf{A}(\mathbf{k}_\perp,\omega)$ gives the amplitude of photoionization with the transverse momentum $\mathbf{k}_\perp$ and its absolute value squared gives the distribution of photoelectrons in $\mathbf{k}_\perp$. Similarly to Eq. (35), we introduce the reduced (this qualification is also omitted below) transverse momentum distribution (TMD),

$$P(\mathbf{k}_\perp,\omega) = |\mathbf{e}\mathbf{A}(\mathbf{k}_\perp,\omega)|^2. \tag{40}$$

This is the second observable to be considered. It is proportional to the distribution of photoelectrons in the transverse plane discussed theoretically in Ref. [17] and measured in Ref. [15].

In the weak-field limit assumed above the solutions of Eq. (24) with $E = E_{\rm in}+\omega$ are almost real, because $E_{\rm in}$ is almost real. Substituting Eq. (39) into Eq. (40) and integrating over $\mathbf{k}_\perp$ using Eq. (26), one obtains that in this case the TMD of photoelectrons and the total photoionization rate are related by

$$\int P(\mathbf{k}_\perp,\omega)\frac{d\mathbf{k}_\perp}{(2\pi)^2} = \gamma(\omega), \tag{41}$$

TABLE I. Energies $\mathcal{E}$ and widths Γ (in atomic units) of the four TSs shown in Fig. 1 at two static-field strengths considered in the calculations.

(n_ξ,n_η,m)	$\mathcal{E}$	Γ	$\mathcal{E}$	Γ
	$F=0.03$		$F=0.10$	
(0,0,0)	−0.502 074	$0.223\,753\times10^{-8}$	−0.527 418	$0.145\,381\times10^{-1}$
(1,0,0)	−0.070 723	$0.665\,210\times10^{-1}$	0.080 235	0.310 374
(0,1,0)	−0.240 147	0.119 640	−0.392 702	0.572 141
(0,0,1)	−0.153 357	$0.888\,472\times10^{-1}$	−0.154 012	0.403 757

which is consistent with their physical meaning. Thus, rates (35) and (36) and TMD (40) provide two complementary sets of characteristics of the photoionization process. We emphasize that the validity of Eq. (41) relies only on the condition that $E_{\rm in}$ is real.

In strong fields the initial-state energy $E_{\rm in}$ acquires a non-negligible imaginary part. As a consequence, the observables discussed above lose their immediate physical meaning and Eq. (41) may hold only approximately. However, these quantities appear in the time-dependent context as characteristics of photoionization in a strong laser field treated within the adiabatic theory [21]. To implement Eqs. (35), (36), and (40) one needs to calculate the coefficients (34). For complex $E_{\rm in}$ the functions $\mathcal{R}_\nu(\eta)$ and $\phi_{\rm in}(\mathbf{r})$ exponentially diverge at $\eta\to\infty$, so the integral over η in Eq. (34) should be regularized. Since $\mathcal{R}_\nu(\eta)$ contains both incoming and outgoing waves at $\eta\to\infty$, the regularization technique differs from that used for the normalization integral (7); it is described in Sec. 3 of the Appendix.

III. RESULTS AND DISCUSSION

We illustrate the theory by calculating photoionization rates (35) and (36) and TMD (40) for the four TSs shown in Fig. 1 at two representative static-field strengths $F=0.03$ and 0.1. The energies and widths of the TSs at these fields are listed in Table I. For a given initial state with the azimuthal quantum number $m_{\rm in}$, the sum over ν in Eqs. (36) and (39) substituted into Eq. (40) contains only channels with $m=m_{\rm in}$, in the LP case, and $m=m_{\rm in}\pm1$, in the CP($\pm$) cases, respectively [see Eq. (15)]. Since the observables have different behavior in the different polarization cases, we consider both linear and circular polarizations for each initial state. In all the cases, the TMD (40) does not depend on the direction of the transverse momentum $\mathbf{k}_\perp$ and is denoted by $P(k_\perp,\omega)$. The complex energy eigenvalues of SFISs the manifestation of which in the photoionization observables we seek are denoted by $E_{n_\xi n_\eta m}=\mathcal{E}_{n_\xi n_\eta m}-\frac{i}{2}\Gamma_{n_\xi n_\eta m}$. Only SFISs with $m=0,1$, and 2 shown in Fig. 1 are involved in the discussion; SFISs with larger m cannot be excited from the initial TSs with $m_{\rm in}=0$ or 1.

We begin with photoionization from the ground TS (0,0,0) by a linearly polarized field. The results are presented in Fig. 2. Let us first consider the lower subpanels. The solid black line shows the total rate (36). The solid color lines show the partial rates (35) with $\nu=(n_\xi,0)$ and $n_\xi=0$ (red), 1 (green), 2 (blue), etc. The leftmost (red) vertical dashed line with a horizontal bar shows the position and width of the TS (0,1,0). The other vertical dashed lines with horizontal bars show the positions and widths of SFISs with $n_\xi=1,2,\ldots$ and $n_\eta=m=0$ (shown in Fig. 1), their colors coinciding with the colors of partial rates with the same n_ξ. The main feature to be noticed in the lower subpanels is that partial rates have well-pronounced broad peaks the positions and widths of which are reproduced by the positions and widths of the corresponding SFISs, and traces of these peaks, and hence SFISs, can be seen also in the total rate. Here we mean the main (leftmost) peaks in each partial rate, which are thus shown to be manifestations of SFISs with $n_\eta=0$. One can notice

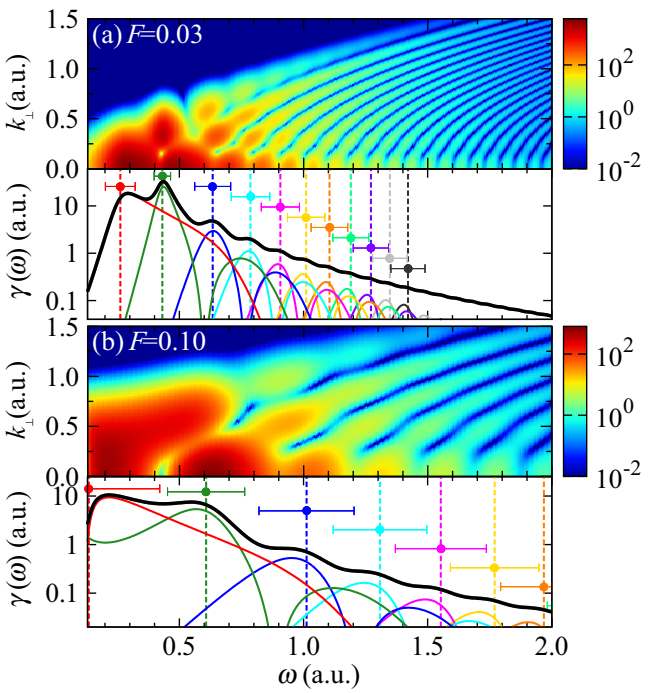

FIG. 2. Characteristics of photoionization from the TS (0,0,0) in a static field of strength (a) $F=0.03$ and (b) $F=0.10$ by a weak monochromatic field of frequency ω in the LP case. The upper subpanels show the TMD $P(k_\perp,\omega)$, Eq. (40). In the lower subpanels, the solid black line shows the total rate $\gamma(\omega)$, Eq. (36); the other solid lines show partial rates $\gamma_\nu(\omega)$, Eq. (35), with $\nu=(n_\xi,0)$, where red, green, blue, etc., colors correspond to $n_\xi=0$, 1, 2, etc., respectively; the leftmost vertical dashed red line shows the TS (0,1,0); the other vertical dashed lines show SFISs $(n_\xi,0,0)$, their colors coinciding with the colors of partial rates with the same n_ξ, that is, green, blue, etc. lines correspond to $n_\xi=1$, 2, etc., respectively. The vertical dashed lines are located at resonance frequencies $\omega=\mathcal{E}_{n_\xi n_\eta m}-\mathcal{E}_{\rm in}$, where $\mathcal{E}_{n_\xi n_\eta m}$ is the energy of the corresponding TS or SFIS, and the horizontal bars indicate the widths of the states.

that partial rates for channels with $n_\xi \geqslant 1$ have secondary lower and broader peaks located at higher frequencies. We have confirmed that positions and widths of these secondary peaks agree with those for SFISs with $n_\eta = 1$ (not shown in the figure). Thus, SFISs with higher n_η manifest themselves in partial rates, but they are too broad and not visible in the total rate. The upper subpanels show color maps of the TMD (40). At low frequencies the TMD has a complex shape determined by an interference of the contributions from the TS (0,1,0) and the lowest SFIS (1,0,0). But at higher frequencies its shape becomes more regular. The TMD as a function of $k_\perp$ at a given ω has a number of oscillations with clearly visible minima and then vanishes as $k_\perp$ grows further. The number depends on ω and is incremented by one as ω passes through a SFIS. The maxima of the TMD seen at such ω at small $k_\perp$ are manifestations of SFISs. The high contrast of the oscillatory pattern of the TMD in the present case is explained by the fact that the initial-state energy $E_{\rm in}$ is almost real, and hence the solutions of Eq. (24) with $E = E_{\rm in} + \omega$ are also almost real and have definite numbers n_ξ of zeros. As can be seen from the plots of partial rates, at each ω the TMD amplitude (39) is given by a superposition of only a few channel functions $\phi_\nu(k_\perp^2/F)$, so it has zeros which are seen as minima lines of the oscillatory pattern. Another consequence of the reality of the solutions of Eq. (24) is that the relation (41) holds well. The integral of the TMD appearing on the left-hand side of this relation is also shown in the lower subpanels of Fig. 2, but this line is indistinguishable from the solid black line showing the total rate. All this holds for both field strengths considered.

Figure 3 presents similar results for photoionization from the same TS (0,0,0), but by a circularly polarized field. In this case, only partial rates for channels with $m = 1$ have nonzero values. They again have peaks the positions and widths of which are in fair agreement with those for SFISs with $n_\eta = 0$ and $m = 1$ (shown in Fig. 1). But the peaks are now too broad and not visible in the total rate, except for the lowest one which originates from the TS (0,0,1). Note that the TMD has a node at $k_\perp = 0$, which is a consequence of the first of the boundary conditions (24b).

We now turn to photoionization from an excited TS (1,0,0) by a linearly polarized field. The results are presented in Fig. 4. The main difference from the previous cases is the appearance of vertical ridges in the TMD at the positions of SFISs (n_ξ,0,0) which are especially pronounced in Fig. 4(b). These ridges have the following origin. As is explained in the end of Sec. II B 2, the Wronskian $\mathcal{W}_\nu$ in Eq. (34) turns to zero whenever the condition $E_{\rm in} + \omega = E_{n_\xi n_\eta m}$ meaning resonance excitation of a SFIS from the initial TS is satisfied. Since ω is real, this condition amounts to the two conditions: $\mathcal{E}_{\rm in} + \omega = \mathcal{E}_{n_\xi n_\eta m}$ and $\Gamma_{\rm in} = \Gamma_{n_\xi n_\eta m}$. The first one can be always satisfied by varying ω; the second one depends only on the field and in some cases (for some initial states) can be satisfied by varying F. Thus, the complex resonance condition can be satisfied at certain combinations of ω and F. When this happens, all the photoionization observables diverge. We mention that in contrast to the elastic-scattering cross section, the value of which is limited by unitarity, the photoionization cross section calculated by treating the electron-photon interaction in the first order of perturbation theory is not restricted by such a condition and, in principle,

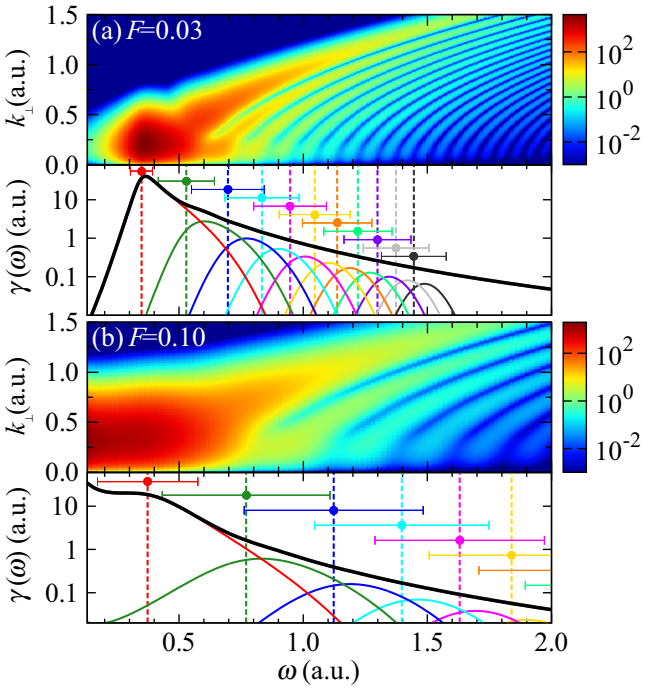

FIG. 3. Similar to Fig. 2, but for photoionization from the TS (0,0,0) in the CP(+) case. In the lower subpanels, solid red, green, blue, etc., lines show partial rates $\gamma_\nu(\omega)$ with $\nu = (n_\xi, 1)$, where n_ξ = 0, 1, 2, etc., respectively; the leftmost vertical dashed red line shows the TS (0,0,1); the other vertical dashed lines show SFISs (n_ξ,0,1), their colors coinciding with the colors of the corresponding partial rates.

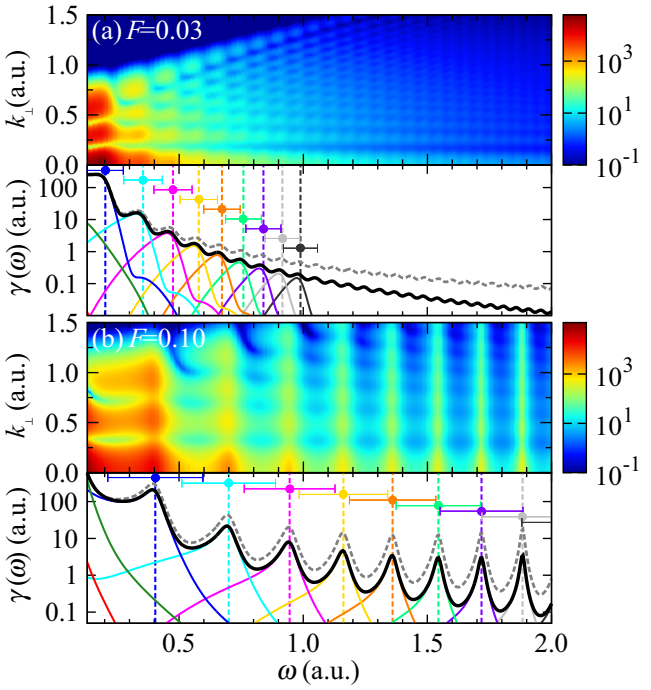

FIG. 4. Characteristics of photoionization from the TS (1,0,0) in the LP case. The dashed gray line in the lower subpanels shows the integral on the left-hand side of Eq. (41). The other notation is as in Fig. 2.

can diverge. Consider, for example, photoionization from a bound state in a potential supporting a very narrow shape resonance of width Γ. The photoionization cross section at the resonance frequency exceeds its off-resonance background value by a factor of $q^2 \propto \Gamma^{-1}$, where q is the Fano parameter [30]. In the limit $\Gamma \to 0$, when the resonance becomes a bound state embedded into the continuum, the cross section acquires a delta-function singularity and diverges. Returning to our discussion, the complex resonance condition is not satisfied for the initial TS (0,0,0), because this state is too narrow compared to SFISs in the interval of fields considered. But this happens in the case shown in Fig. 4, because the width of the TS (1,0,0), see Table I, is comparable to those of SFISs. Since we consider only two discrete values of F, the resonance condition is not satisfied exactly, but one can see resonance enhancement of the observables at the positions of SFISs. The value of $\Gamma_{\rm in}$ is closer to $\Gamma_{n_\xi n_\eta m}$ for SFISs with higher n_ξ at the stronger field $F = 0.1$, so the resonance enhancement in this case is more pronounced. Notice that the widths of peaks in partial rates in Fig. 4(a) correspond to the widths of SFISs, but in Fig. 4(b) the peaks are much narrower. This is because their actual widths in the latter case are determined by the resonance enhancement, that is, by the difference $|\Gamma_{n_\xi n_\eta m} - \Gamma_{\rm in}|$ instead of the SFIS's width $\Gamma_{n_\xi n_\eta m}$ alone. The large width of the present initial state also explains the disappearance of the oscillatory pattern of the TMD, which was the dominant feature in Figs. 2 and 3. Some traces of the pattern still can be seen, but its contrast is greatly reduced. For the same reason the relation (41) does not hold well anymore: the dashed gray line showing the integral on the left-hand side of this relation now is easily distinguishable from the solid black line showing the right-hand side, and the difference grows with ω.

Figure 5 presents results for photoionization from the same TS (1,0,0), but by a circularly polarized field. In this case, the initial TS is much narrower than SFISs (n_ξ,0,1), so no resonance enhancement occurs. Peaks of partial rates are too broad and not visible in the total rate. The TMD has almost no structure; only a low-contrast oscillatory pattern similar to that in Figs. 2 and 3 can be seen.

Figures 6 and 7 are similar to Figs. 4 and 5, respectively, but for photoionization from another excited TS (0,1,0). The resonance enhancement of the manifestations of SFISs in this case is even more pronounced and can be seen also for the stronger field in the CP(+) case [see Fig. 7(b)]. This means that even very broad SFISs can be made visible in photoionization observables at appropriate frequencies by properly choosing the field. One new feature can be noticed in Fig. 6(b): the total rate $\gamma(\omega)$ (solid black line) has a small sharp peak at $\omega \approx 1.4$ originating from the partial rate with $n_\xi = 2$ (solid blue line). This peak is explained as follows. The different separation constant eigenvalues β_ν of Eq. (24) represent different branches of a single multivalued analytic function of E. The branches are connected by branch points. One of them connecting states with $\nu = (2,0)$ and (3,0) is located at $E_{\rm BP} = (1.006\,919, -0.285\,660)$. Its imaginary part happened to be very close to $-\Gamma_{\rm in}/2 \approx -0.286\,071$ at $F = 0.1$, see Table I, so at $\omega = 1.399\,621$ we have $E_{\rm in} + \omega \approx E_{\rm BP}$. Thus, the sharp peak in Fig. 6(b) is a manifestation of the branch point of the separation constant β_ν. Many other such branch points can be found by varying F.

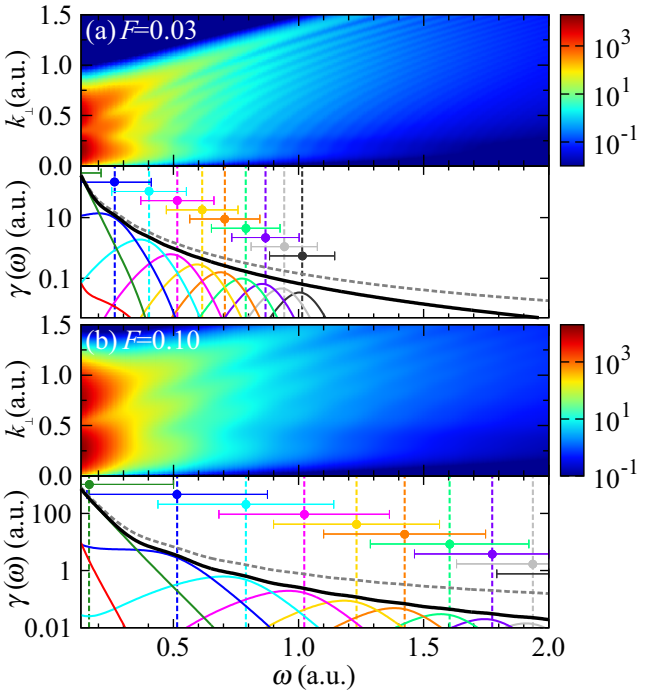

FIG. 5. Characteristics of photoionization from the TS (1,0,0) in the CP(+) case. The dashed gray line in the lower subpanels shows the integral on the left-hand side of Eq. (41). The other notation is as in Fig. 3.

We finally consider photoionization from the lowest TS (0,0,1) with nonzero azimuthal quantum number. The results in the LP, CP(−), and CP(+) cases are presented in Figs. 8, 9, and 10, respectively. The figures show partial rates and SFISs

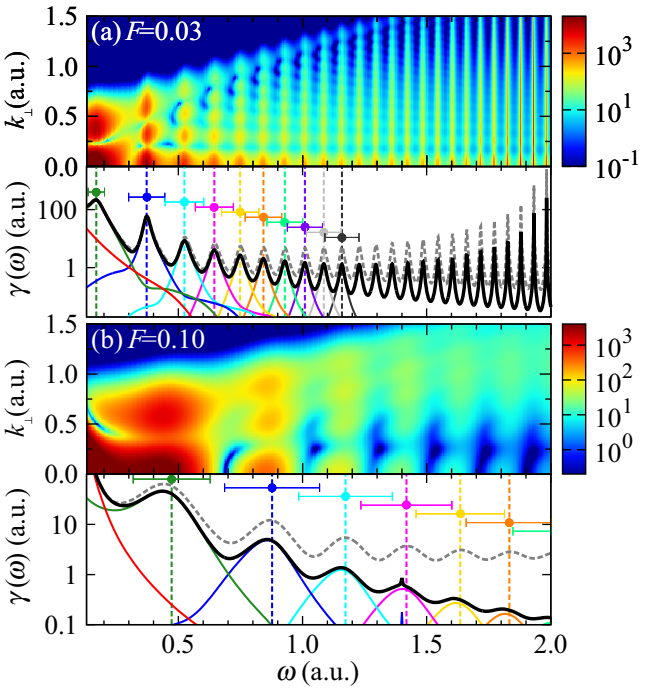

FIG. 6. Characteristics of photoionization from the TS (0,1,0) in the LP case. The notation is as in Figs. 2 and 4.

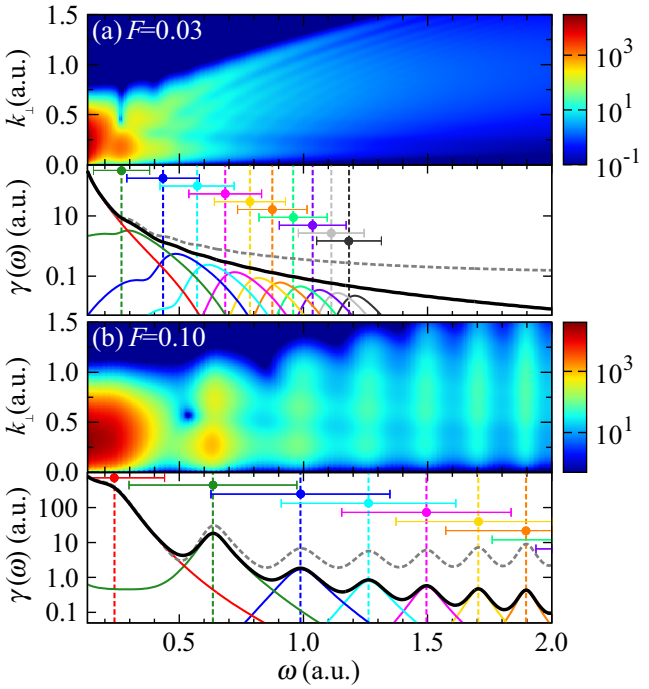

FIG. 7. Characteristics of photoionization from the TS (0,1,0) in the CP(+) case. The notation is as in Figs. 3 and 5.

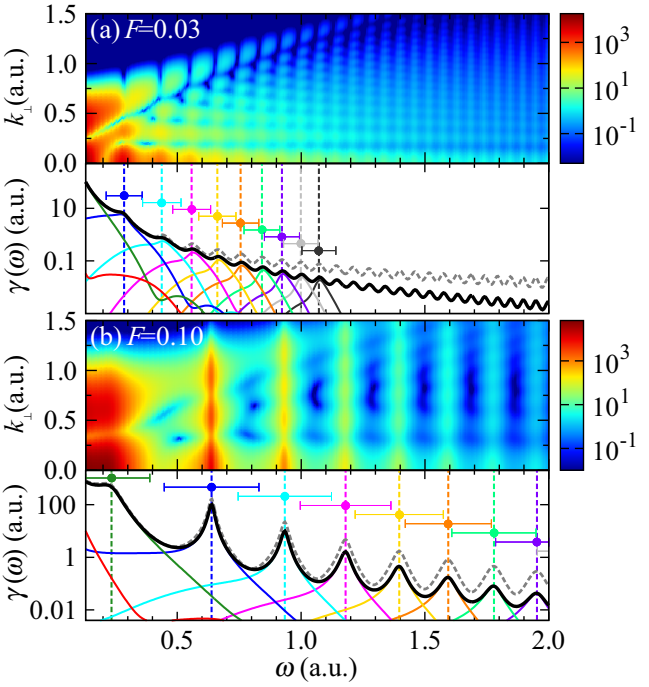

FIG. 9. Characteristics of photoionization from the TS (0,0,1) in the CP(−) case. The notation is as in Figs. 2, 4, and 6.

with $m = 1$, 0, and 2, respectively. The width of the initial TS in the present case is comparable to those of SFISs with $m = 0$, which is why we see strong resonance enhancement of the manifestations of SFISs in Fig. 9. SFISs with $m = 1$ are broader, but their traces still can be seen in the total rate

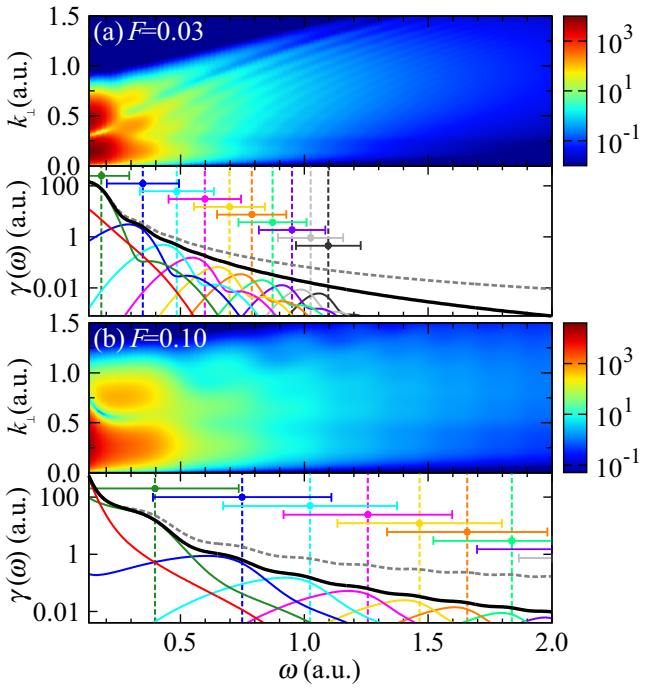

FIG. 8. Characteristics of photoionization from the TS (0,0,1) in the LP case. The notation is as in Figs. 3, 5, and 7.

in Fig. 8(b). SFISs with $m = 2$ are even broader and do not reveal themselves in Fig. 10.

The most interesting feature of the results presented in Figs. 2–10 is that peaks manifesting SFISs in photoionization observables due to the resonance enhancement at some field strengths become narrow and very well pronounced even for broad SFISs. To further illustrate this feature and make it more clear, we return to photoionization from the TS (0,1,0) by a linearly polarized field (see Fig. 6). We have calculated the total rate $\gamma(\omega)$ in this case as a function of ω and continuously varied F; the results are presented in Fig. 11. The vertical axis in the figure is related to ω by $\mathcal{E} = \mathcal{E}_{\rm in} + \omega$. The cuts of this figure at $F = 0.03$ and 0.1 are shown by solid black lines in Fig. 6. One can clearly see ridges following the positions of SFISs $(n_\xi,0,0)$, along which the values of $\gamma(\omega)$ are resonantly enhanced. The ridges are much narrower than the SFISs. The complex resonance condition $E_{\rm in} + \omega = E_{n_\xi 00}$ is exactly satisfied at some points (shown by solid black circles) at the ridges, and $\gamma(\omega)$ diverges at these points. Note that the other TS (1,0,0) shown in Fig. 11 also causes resonance enhancement of the rate, but the exact resonance is never achieved in this case, because at all fields the TS (0,1,0) remains broader than the TS (1,0,0).

To conclude the discussion, it is worthwhile to mention that there exists a different language which may be found useful for interpreting the above results. In Ref. [8], the field-induced structure of photoionization cross sections in a static electric field was interpreted as interference of classical trajectories. The argumentation proceeds as follows. Suppose there is an isotropic source of electrons with energy $E = k^2/2$ located at the origin. For simplicity, we consider only the motion along the field. Electrons emitted towards $z > 0$ are reflected by the field, return to the origin, and interfere with electrons emitted

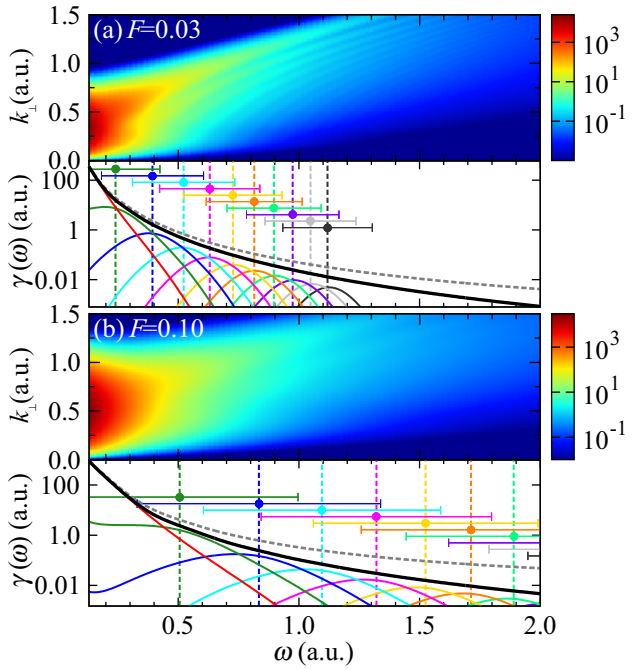

FIG. 10. Characteristics of photoionization from the TS (0,0,1) in the CP(+) case. In the lower subpanels, solid red, green, blue, etc., lines show partial rates $\gamma_\nu(\omega)$ with $\nu = (n_\xi,2)$, where $n_\xi = 0$, 1, 2, etc., respectively; vertical dashed lines show SFISs $(n_\xi,0,2)$, their colors coinciding with the colors of partial rates with the same n_ξ. The other notation is as in previous figures.

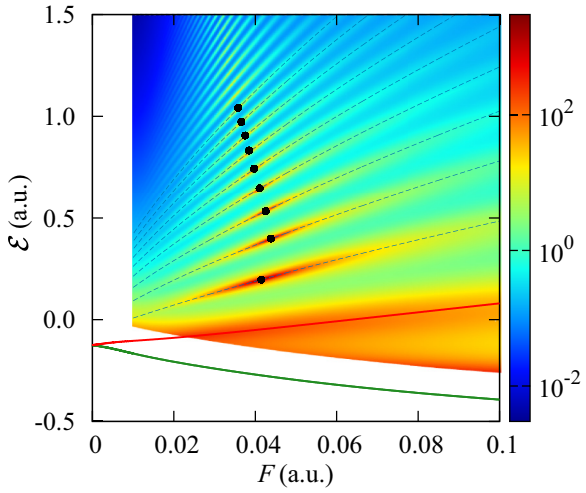

FIG. 11. Solid green and red lines show real parts of the energies of the TSs (0,1,0) and (1,0,0), respectively, as in Fig. 1. Dashed lines show real parts of the energies of SFISs $(n_\xi,0,0)$ with $n_\xi = 2,\ldots,10$ (from bottom to top) also shown in Fig. 1. The color map shows the total rate $\gamma(\omega)$ of photoionization from the TS (0,1,0) by a linearly polarized field, where $\omega = \mathcal{E} - \mathcal{E}_{\rm in}$. Solid black circles indicate points where the complex resonance condition $E_{\rm in} + \omega = E_{n_\xi 00}$ is satisfied for the different SFISs, and therefore the rate diverges.

towards $z < 0$. The additional action accumulated by the former electrons is $\Delta S = 2k^3/3F$. The constructive interference occurs when $\Delta S = 2\pi n, n = 1,2,\ldots$, so the amplitude of the outgoing flux as a function of E oscillates attaining maxima when $k^3/3F = \pi n$ [8]. This argumentation suggests a very simple and attractive picture which qualitatively explains both the appearance of peaks in the photoionization cross section [8] and the principles of operation of the photoionization microscope [20]. This picture can be also used to interpret the present results. For example, the absence of structure in $\gamma(\omega)$ for photoionization from an initial state with $m_{\rm in} = 0$ by a circularly polarized field seen in Figs. 3 and 5 and the upper panel of Fig. 7 can be interpreted as the absence of the returning trajectory which exists and interferes with the direct trajectory in the LP case. However, the applicability of such an interpretation is limited: the rate $\gamma(\omega)$ may have peaks even in the absence of the returning trajectory, as is the case in the lower panel of Fig. 7. The main deficiency of the picture of interfering trajectories proposed in Ref. [8] is that it does not account for the atomic potential. The incorporation of the Coulomb potential into this picture for the case of weak fields considered in Ref. [11] makes it more adequate, but at the same time not that simple anymore. The same applies to strong fields considered in the present paper. Indeed, the quantization condition for SFISs (10) was derived under the assumption $k^3/3F \gg 1$ [22], which corresponds to large n_ξ. In this case one can approximately neglect all but the first terms on the left- and right-hand sides of Eq. (10). The resulting equation $k^3/3F = \pi n_\xi$ does not contain any information about the potential and coincides with the condition obtained in Ref. [8]. However, Eq. (10) was shown to closely reproduce the exact energies of SFISs [22], on the one hand, and the positions of the peaks of $\gamma(\omega)$ seen in Figs. 4, 6, 7, and 9 are in excellent agreement with the energies of SFISs, on the other hand. Thus, the potential-dependent terms in Eq. (10) are essential for describing the peaks quantitatively.

IV. CONCLUSIONS AND PERSPECTIVES

In this paper we have extended previous theoretical studies of photoionization of hydrogen in a static electric field [7–11,17] to much stronger fields of order $F \sim 0.1$, which is of interest for strong-field physics. At such fields even the ground state acquires a non-negligible width, so one should treat photoionization from a decaying initial TS. We have defined appropriate photoionization observables—the reduced photoionization rate and transverse momentum distribution of photoelectrons. The main conclusion of the paper is that SFISs found in Ref. [22] do manifest themselves as distinct peaks in the observables. The widths of the peaks are determined by the difference between the widths of the SFISs and that of the initial TS, not by the widths of the SFISs alone. As a result, the peaks are resonantly enhanced at some fields and become narrow and very well pronounced even for broad SFISs. We emphasize that such a resonance enhancement of the manifestations of SFISs is possible only due to complexity of the energy of the initial TS; this mechanism could not be found in the previous studies [7–11,17], which treated photoionization from an unperturbed bound state. A decaying TS cannot be probably prepared as an initial state for photoionization experiment in a truly static field $F \sim 0.1$, because it rapidly decays and such static fields are not currently available. But it can be prepared by the interaction with a

strong low-frequency laser field in the adiabatic regime [21]. Within the adiabatic theory [21], photoionization observables in a quasistatic laser field can be expressed in terms of their static-field counterparts studied in this paper. Thus, we expect that SFISs should also manifest themselves in photoionization by a weak probe pulse in the presence of a quasistatic field of a strong pump pulse. The study in this direction is in progress.

ACKNOWLEDGMENTS

This work was supported in part by Japan Society for the Promotion of Science KAKENHI Grants No. 26400415, No. 16H04029, and No. 16H04103. S.O. is grateful to Moscow Institute of Physics and Technology for financial support and hospitality during his visit under the internship program. O.I.T. acknowledges support from the Ministry of Education and Science of Russia (State Assignment No. 3.873.2017).

APPENDIX: NUMERICAL PROCEDURE

1. Siegert states

To construct hydrogenic SSs one has to solve Eqs. (4) and (5). We expand the solutions of Eqs. (4) in a basis consisting of the solutions for $F = 0$. The basis functions are known analytically [28] and expressed in terms of the generalized Laguerre polynomials $L_{n_\xi}^{(|m|)}(\xi)$ [29]. Substituting the expansion into Eq. (4a) turns it into an algebraic eigenvalue problem with five-diagonal matrix. The same basis is used for solving Eqs. (5), but prior to expanding the solution the real η axis is rotated upwards in the complex η plane. The expansion is applied at the ray $\arg\eta = \pi/3$ along which the outgoing-wave solutions satisfying Eq. (5b) exponentially decay, and hence can be expanded in a square integrable basis. Thus, Eq. (5a) is also turned into an algebraic eigenvalue problem with five-diagonal matrix. Each of these problems can be solved by means of standard linear algebra packages. Their simultaneous solutions can be found iteratively, with the initial guesses for the energy E and separation constant β eigenvalues at weak fields provided by the field-free hydrogenic energies and Eq. (9), for TSs, and by the asymptotic quantization condition derived in Ref. [22] and Eq. (11), for SFISs. Once a solution is found for one value of F, it can be analytically continued to stronger or weaker fields by making small steps in F. The results were controlled by comparing with calculations by another method, which enables one to construct SSs for arbitrary spherically symmetric potentials [23].

2. Green's function

The solutions of Eqs. (24) can be obtained in the same way as we solve Eqs. (4). This defines the separation constants β_ν for a given E. To implement Eq. (34) we additionally need the regular solution $\mathcal{R}_\nu(\eta)$ of the homogeneous version of Eq. (27). To construct this function, we divide the η axis into three parts. In the inner interval, $0 \leqslant \eta \leqslant \eta_0$, we expand the solution in the form

$$\mathcal{R}_\nu(\eta) = \eta^{(1+|m|)/2} \sum_n a_n \eta^n, \tag{A1}$$

where the coefficients are given by

$$a_0 = 1, \quad a_1 = -\frac{\beta_\nu a_0}{1+|m|}, \tag{A2a}$$

$$a_2 = -\frac{\beta_\nu a_1 + \frac{1}{2}E a_0}{2(2+|m|)}, \tag{A2b}$$

$$a_{n\geqslant 3} = -\frac{\beta_\nu a_{n-1} + \frac{1}{2}E a_{n-2} + \frac{1}{4}F a_{n-3}}{n(n+|m|)}. \tag{A2c}$$

In the intermediate interval, $\eta_0 \leqslant \eta \leqslant \eta_1$, we solve the equation numerically by the standard fourth-order Runge-Kutta method [31]. In the outer interval, $\eta_1 \leqslant \eta$, we express the regular solution in terms of the incoming $(-)$ and outgoing $(+)$ solutions,

$$\mathcal{R}_\nu(\eta) = \frac{\mathcal{W}_\nu}{2i}[f_\nu^{(-)}(\eta,E) - i e^{2i\delta_\nu} f_\nu^{(+)}(\eta,E)], \tag{A3}$$

which are given by the asymptotic expansions

$$f_\nu^{(\pm)}(\eta,E) = \frac{2^{1/2}}{(F\eta)^{1/4}} \exp\left(\pm\frac{iF^{1/2}\eta^{3/2}}{3} \pm \frac{iE\eta^{1/2}}{F^{1/2}}\right) \times \sum_n \frac{f_n^{(\pm)}}{\eta^{n/2}} \tag{A4}$$

with the coefficients

$$f_0^{(\pm)} = 1, \quad f_1^{(\pm)} = \pm\frac{4\beta_\nu - E^2F^{-1}}{2iF^{1/2}} f_0^{(\pm)}, \tag{A5a}$$

$$f_2^{(\pm)} = \pm\frac{(4\beta_\nu - E^2F^{-1})f_1^{(\pm)} \mp 2iEF^{-1/2} f_0^{(\pm)}}{4iF^{1/2}}, \tag{A5b}$$

$$f_{n\geqslant 3}^{(\pm)} = \pm\frac{(4\beta_\nu - E^2F^{-1})f_{n-1}^{(\pm)} \mp 2iEF^{-1/2}(n-1)f_{n-2}^{(\pm)} + [(n-3)n + 9/4 - m^2]f_{n-3}^{(\pm)}}{2inF^{1/2}}. \tag{A5c}$$

By matching the solution obtained in the intermediate interval at η_1 with that given by Eqs. (A3)–(A5), we find the Wronskian $\mathcal{W}_\nu$ and the phase shift δ_ν.

3. The integral in Eq. (34)

Next we describe the numerical technique for calculating the integral in Eq. (34). The initial SS is obtained in the form [see Eq. (3)]

$$\phi_{\rm in}(\mathbf{r}) = \eta^{-1/2} f_{\rm in}(\eta)\phi_{\rm in}(\xi)\frac{e^{im_{\rm in}\varphi}}{\sqrt{2\pi}}. \tag{A6}$$

Substituting this into Eq. (34), we obtain the Cartesian components of $\mathbf{d}_\nu(\omega)$:

$$d_{\nu x}(\omega) = \frac{1}{4\mathcal{W}_\nu}(\delta_{m,m_{\rm in}+1} + \delta_{m,m_{\rm in}-1})\big[I_\nu^{(3/2)}J_\nu^{(-1/2)} + I_\nu^{(1/2)}J_\nu^{(1/2)}\big], \tag{A7a}$$

$$d_{\nu y}(\omega) = \frac{1}{4i\mathcal{W}_\nu}(\delta_{m,m_{\rm in}+1} - \delta_{m,m_{\rm in}-1})\big[I_\nu^{(3/2)}J_\nu^{(-1/2)} + I_\nu^{(1/2)}J_\nu^{(1/2)}\big], \tag{A7b}$$

$$d_{\nu z}(\omega) = \frac{1}{4\mathcal{W}_\nu}\delta_{m,m_{\rm in}}\big[I_\nu^{(2)}J_\nu^{(-1)} - I_\nu^{(0)}J_\nu^{(1)}\big], \tag{A7c}$$

where

$$I_\nu^{(k)} \equiv \int_0^\infty \xi^k \phi_\nu(\xi)\phi_{\rm in}(\xi)\,d\xi \tag{A8}$$

and

$$J_\nu^{(k)} \equiv \int_0^\infty \eta^k \mathcal{R}_\nu(\eta) f_{\rm in}(\eta)\,d\eta. \tag{A9}$$

The functions $\phi_\nu(\xi)$ and $\phi_{\rm in}(\xi)$ are given by expansions in Laguerre basis, so the integrals (A8) can be calculated analytically. The integration in Eq. (A9) over the inner $0 \leqslant \eta \leqslant \eta_0$ and intermediate $\eta_0 \leqslant \eta \leqslant \eta_1$ intervals is performed along the real axis. The integration over the outer interval $\eta_1 \leqslant \eta$ is more tricky, because both functions $\mathcal{R}_\nu(\eta)$ and $f_{\rm in}(\eta)$ exponentially diverge as $\eta \to \infty$ along the real axis. We regularize this integral as follows. The function $\mathcal{R}_\nu(\eta)$ is presented by Eq. (A3). Its incoming $(-)$ and outgoing $(+)$ parts are integrated along rays obtained by rotating the real ray $[\eta_1,\infty)$ downwards and upwards in the complex η plane, respectively. The rotation angle is chosen to ensure convergence and is $\sim\pi/3$.

[1] R. R. Freeman, N. P. Economou, G. C. Bjorklund, and E. T. Lu, Observation of Electric-Field-Induced Resonances above the Ionization Limit in a One-Electron Atom, Phys. Rev. Lett. **41**, 1463 (1978).

[2] R. R. Freeman and N. P. Economou, Electric field dependence of the photoionization cross section of Rb, Phys. Rev. A **20**, 2356 (1979).

[3] W. L. Glab and M. H. Nayfeh, Stark-induced resonances in the photoionization of hydrogen, Phys. Rev. A **31**, 530 (1985).

[4] W. L. Glab, K. Ng, D. Yao, and M. H. Nayfeh, Spectroscopy between parabolic states in hydrogen: Enhancement of the Stark-induced resonances in its photoionization, Phys. Rev. A **31**, 3677 (1985).

[5] H. Rottke and K. H. Welge, Photoionization of the hydrogen atom near the ionization limit in strong electric fields, Phys. Rev. A **33**, 301 (1986).

[6] F. Krausz and M. Ivanov, Attosecond physics, Rev. Mod. Phys. **81**, 163 (2009).

[7] V. D. Kondratovich and V. N. Ostrovski, Photoionization of a hydrogenlike atom in a homogeneous electric field, Zh. Eksp. Teor. Fiz. **79**, 395 (1980) [Sov. Phys. JETP **52**, 198 (1981)].

[8] I. I. Fabrikant, Interference effects in photodetachment and photoionization of atoms in a homogeneous electric field, Zh. Eksp. Teor. Fiz. **79**, 2070 (1980) [Sov. Phys. JETP **52**, 1045 (1981)].

[9] E. Luc-Koenig and A. Bachelier, Systematic theoretical study of the Stark spectrum of atomic hydrogen I: Density of continuum states, J. Phys. B **13**, 1743 (1980).

[10] D. A. Harmin, Hydrogenic Stark effect: Properties of the wave functions, Phys. Rev. A **24**, 2491 (1981).

[11] V. D. Kondratovich and V. N. Ostrovski, Resonance and interference phenomena in the photoionisation of a hydrogen atom in a uniform electric field: II. Overlapping resonances and interference, J. Phys. B **17**, 2011 (1984).

[12] V. V. Kolosov, Long-lived Stark states detected at a positive energy, Pis'ma Zh. Eksp. Teor. Fiz. **44**, 457 (1986) [Sov. Phys. JETP Lett. **44**, 588 (1986)].

[13] S. Cohen, M. M. Harb, A. Ollagnier, F. Robicheaux, M. J. J. Vrakking, T. Barillot, F. Lépine, and C. Bordas, Wave Function Microscopy of Quasibound Atomic States, Phys. Rev. Lett. **110**, 183001 (2013).

[14] S. Cohen, M. M. Harb, A. Ollagnier, F. Robicheaux, M. J. J. Vrakking, T. Barillot, F. Lépine, and C. Bordas, Photoionization microscopy of the lithium atom: Wave-function imaging of quasibound and continuum Stark states, Phys. Rev. A **94**, 013414 (2016).

[15] A. S. Stodolna, A. Rouzée, F. Lépine, S. Cohen, F. Robicheaux, A. Gijsbertsen, J. H. Jungmann, C. Bordas, and M. J. J. Vrakking, Hydrogen Atoms under Magnification: Direct Observation of the Nodal Structure of Stark States, Phys. Rev. Lett. **110**, 213001 (2013).

[16] A. S. Stodolna, F. Lépine, T. Bergeman, F. Robicheaux, A. Gijsbertsen, J. H. Jungmann, C. Bordas, and M. J. J. Vrakking, Visualizing the Coupling between Red and Blue Stark States Using Photoionization Microscopy, Phys. Rev. Lett. **113**, 103002 (2014).

[17] L. B. Zhao and J. B. Delos, Dynamics of electron wave propagation in photoionization microscopy. II. Quantum-mechanical formulation, Phys. Rev. A **81**, 053418 (2010).

[18] L. B. Zhao, I. I. Fabrikant, J. B. Delos, F. Lépine, S. Cohen, and C. Bordas, Coupled-channel theory of photoionization microscopy, Phys. Rev. A **85**, 053421 (2012).

[19] L. B. Zhao, I. I. Fabrikant, M. L. Du, and C. Bordas, Test of the Stark-effect theory using photoionization microscopy, Phys. Rev. A **86**, 053413 (2012).

[20] Yu. N. Demkov, V. D. Kondratovich, and V. N. Ostrovski, Interference of electrons resulting from the photoionization of an atom in an electric field, Pis'ma Zh. Eksp. Teor. Fiz. **34**, 425 (1981) [Sov. Phys. JETP Lett. **34**, 403 (1981)].

[21] O. I. Tolstikhin and T. Morishita, Adiabatic theory of ionization by intense laser pulses: Finite-range potentials, Phys. Rev. A **86**, 043417 (2012).

[22] A. V. Gets and O. I. Tolstikhin, Static-field-induced states, Phys. Rev. A **87**, 013419 (2013).

[23] P. A. Batishchev, O. I. Tolstikhin, and T. Morishita, Atomic Siegert states in an electric field: Transverse momentum distribution of the ionized electrons, Phys. Rev. A **82**, 023416 (2010).

[24] L. D. Landau and E. M. Lifshitz, *Quantum Mechanics (Non-Relativistic Theory)* (Pergamon, Oxford, 1977).

[25] S. Yu. Slavyanov, Application of the method of standard comparison problems to perturbations of the Coulomb field. The discrete spectrum, Probl. Mat. Fiz. **4**, 125 (1970) [*Topics in Mathematical Physics* (Consultants Bureau, New York, 1971), Vol. 4, p. 113].

[26] T. Yamabe, A. Tachibana, and H. J. Silverstone, Theory of the ionization of the hydrogen atom by an external electrostatic field, Phys. Rev. A **16**, 877 (1977).

[27] T. P. Grozdanov, P. S. Krstić, M. J. Raković, and E. A. Solov'ev, On broad resonances in the hydrogenic Stark effect, Phys. Lett. A **132**, 262 (1988).

[28] O. I. Tolstikhin, T. Morishita, and L. B. Madsen, Theory of tunneling ionization of molecules: Weak-field asymptotics including dipole effects, Phys. Rev. A **84**, 053423 (2011).

[29] *Handbook of Mathematical Functions*, edited by M. Abramowitz and I. A. Stegun (Dover, New York, 1972).

[30] U. Fano, Effects of configuration interaction on intensities and phase shifts, Phys. Rev. **124**, 1866 (1961).

[31] W. H. Press, S. A. Teukolsky, W. T. Vetterling, and B. P. Flannery, *Numerical Recipes in FORTRAN* (Cambridge University, Cambridge, England, 1992).